Vertical Heat Transport by Ocean Circulation and the Role of Mechanical and Haline Forcing

Author:
Zika, J; Sijp, Willem; England, Matthew

Publication details:
Journal of Physical Oceanography
v. 43
Chapter No. 10
pp. 2095-2112
0022-3670 (ISSN)

Publication Date:
2013

Publisher DOI:
http://dx.doi.org/10.1175/JPO-D-12-0179.1

Vertical Heat Transport by Ocean Circulation and the Role of Mechanical and Haline Forcing

JAN D. ZIKA

ARC Centre of Excellence for Climate System Science, University of New South Wales, Sydney, New South Wales, Australia, and National Oceanography Centre, University of Southampton, Southampton, United Kingdom

WILLEM P. SIJP AND MATTHEW H. ENGLAND

ARC Centre of Excellence for Climate System Science, University of New South Wales, Sydney, New South Wales, Australia

(Manuscript received 29 August 2012, in final form 23 May 2013)

ABSTRACT

Vertical transport of heat by ocean circulation is investigated using a coupled climate model and novel thermodynamic methods. Using a streamfunction in temperature–depth coordinates, cells are identified by whether they are thermally direct (flux heat upward) or indirect (flux heat downward). These cells are then projected into geographical and other thermodynamic coordinates. Three cells are identified in the model: a thermally direct cell coincident with Antarctic Bottom Water, a thermally indirect deep cell coincident with the upper limb of the meridional overturning circulation, and a thermally direct shallow cell coincident with the subtropical gyres at the surface. The mechanisms maintaining the thermally indirect deep cell are investigated. Sinking water within the deep cell is more saline than that which upwells, because of the coupling between the upper limb and the subtropical gyres in a broader thermohaline circulation. Despite the higher salinity of its sinking water, the deep cell transports buoyancy downward, requiring a source of mechanical energy. Experiments run to steady state with increasing Southern Hemisphere westerlies show an increasing thermally indirect circulation. These results suggest that heat can be pumped downward by the upper limb of the meridional overturning circulation through a combination of salinity gain in the subtropics and the mechanical forcing provided by Southern Hemisphere westerly winds.

1. Vertical transport in the ocean

The ocean plays a crucial role in regulating the earth's climate, with the upper 2.5 m of the ocean able to store as much heat as the entire atmosphere (Gill 1982). Over the past half century, the ocean has absorbed more than 5 times as much heat as all the other components of the earth system combined (Solomon et al. 2007). Ocean warming has caused a significant fraction of global sea level rise over the past half century (Domingues et al. 2008). Heat absorbed by the ocean today can take centuries to be rereleased into the atmosphere (Held et al. 2010) and is dependent on ocean ventilation time scales (England 1995). Regardless of future climate forcing scenarios, any warming of the ocean today may maintain a significant fraction of established global temperature changes into the foreseeable future.

Despite its importance in the global climate system, little attention has been directed toward understanding vertical heat transport in the ocean. In fact, the term ''ocean heat transport'' has become synonymous with meridional transport of heat by the ocean (Jayne and Marotzke 2002; Ferrari and Ferreira 2011).

Classical models of ocean circulation assume that heat is fluxed downward by small-scale mixing, balancing a thermally direct overturning circulation that fluxes heat upward through upwelling of warm water and downwelling of cold water (Munk 1966; Stommel and Arons 1960; Sandström 1908). In this paradigm, heat uptake by the deep ocean would be set by the vertical temperature gradient and vertical mixing rather than circulation. Subsequent authors have queried this view, proposing that the overturning circulation of the upper 2000 m is set by Southern Hemisphere winds as a result of the Drake Passage effect (Toggweiler and Samuels 1995).

Corresponding author address: Jan D. Kika, University of Southampton, National Oceanography Centre, European Way, Southampton, SO14 3ZH, United Kingdom.
E-mail: J.D.Zika@soton.ac.uk

DOI: 10.1175/JPO-D-12-0179.1

The Drake Passage in the Southern Ocean and its consequent Antarctic Circumpolar Current permits global circulation in the upper 2000 m of the ocean without vertical mixing. If circulation were truly adiabatic, cold water that downwells in the North Atlantic would upwell in the Southern Ocean at the same temperature, leading to no net vertical transport of heat. As such, adiabatic theories suggest that general circulation could play a minor role in transporting heat downward or upward in the ocean.

Recent studies by Gnanadesikan et al. (2005) and Gregory (2000) have cast new light on the mechanisms of vertical heat transport operating in ocean models. Gnanadesikan et al. (2005) and Gregory (2000) find that heat is, in fact, advected downward into the deep ocean and mixed upward in the upper 2000 m of coarse-resolution climate models. That is, they find circulation of the upper ocean to be apparently thermally indirect.

How the different components of ocean circulation such as subtropical gyres, deep overturning, and abyssal Antarctic Bottom Water (AABW) circulation flux heat vertically is an open question. Nycander et al. (2007) and Nurser and Lee (2004) present a novel formalism in this regard. They average the vertical transport in depth–density coordinates. In such coordinates, cells that flux dense water downward are thermally direct and cells that flux less-buoyant water downward are thermally indirect. Nycander et al. (2007) link thermally direct cells to buoyant processes and link thermally indirect cells to mechanical processes.

Nycander et al. (2007) identify three distinct cells in an eddy permitting ocean model. They are (i) a thermally direct dense bottom cell stretching from the surface to around 5000-m depth, (ii) a thermally indirect deep cell reaching from the surface to 2000-m depth, and (iii) a thermally direct light surface cell occupying only the upper 500 m of the ocean. It is as yet unclear, however, how the three thermodynamically distinct cells of Nycander et al. (2007) are connected to geographically distinct components of circulation such as the subtropical gyres and the deep overturning circulation.

As previous authors have shown (Ferrari and Ferreira 2011; Nycander et al. 2007; Zika et al. 2012; Döös et al. 2012), understanding the way the ocean transports heat depends critically on the way in which ocean transport is averaged. In this study, we aim to advance the averaging methods proposed by those authors and to use such methods to diagnose the mechanisms by which ocean circulation transports heat vertically in a climate model.

We will start in section 2 with a review of recent advances in our understanding and diagnosis of residual circulation. The intermediate complexity ocean model used in this study is described in section 3. In section 4, the vertical transport of the model is considered in temperature–depth coordinates and we confirm that three distinct cells exist in the model. In section 5, the three cells are projected into geographical coordinates, and in section 6 each cell is projected into salinity and density coordinates. How the different cells exchange salt within a broader thermohaline circulation is explored in section 7 by projecting the thermal overturning cells into thermohaline (temperature–salinity) coordinates. In section 8, the role of wind forcing in ultimately driving the thermally direct component of circulation is supported via wind perturbation experiments. Section 9 contains a discussion and concluding remarks are made in section 10.

2. The residual circulation

Throughout the ocean, tides, waves, and coherent recirculations move waters of different temperatures and salinities to and fro with instantaneous velocities ranging between millimeters and meters per second. Such flows can amount to very little net transport of heat or salt across latitude lines or through constant depth surfaces. Meanwhile, a background residual circulation transports properties meridionally and vertically and is characterized by velocities on the order of millimeters per second (meridionally) and micrometers per second (vertically). A common way of understanding the residual circulation is to consider a layer bounded by two surfaces of constant density from ρ to $\rho + \Delta\rho$ with a thickness h. Averaging the velocity v within the isopycnal layer, one obtains the total transport of water within that layer $\overline{vh}$ (McDougall and McIntosh 1996). There may be zero mean northward velocity at constant depth ($\overline{v} = 0$) and yet a net transport may exist within an isopycnal layer.

Consider flow through a narrow channel separating two seas. Cold dense water may flow out through a channel in winter and warm light water may flow in through the channel in summer. The net transport at constant density is thus nonzero. However, if the in- and outflow occur at the same depth, the transport averaged at constant depth will be zero. Alternatively, the flow may come in and out at the same density but at different depths. Thus there will be a very large mean velocity at a particular depth, but no transport at constant density. More generally then $\overline{vh} \neq \overline{v}\,\overline{h}$. Thus, the following Reynolds decomposition is required:

$$\overline{vh} = \overline{v}\,\overline{h} + \overline{v'h'}, \tag{1}$$

where v' and h' are perturbations to the mean. The mean here can be spatial, in which case $\overline{v'h'}$ is due to deviations in the spatial mean, or temporal, in which case $\overline{v'h'}$ is due

to deviations in the temporal mean. More precisely, the mean depends on the averaging operator used. Dividing the transport within a layer by the mean thickness of that layer yields a residual velocity $\overline{vh}/\overline{h}$, which is representative of the total transport of mass. Alternative forms of the residual velocity are defined by averaging the mass transport at constant depth to form a transformed Eulerian mean velocity (Andrews and McIntyre 1976). Such a formalism has been extended to any tracer variable and described as the generalized transformed Eulerian mean (Eden et al. 2007).

Recently, Pauluis et al. (2011) revisit the concept of a residual transport, posing the problem in terms of a distribution function M. For some time-evolving scalar variable $C(x, y, z, t)$, one can compute a distribution function M_C^y describing the transport in the y direction at concentration C^* such that

$$M_C^y(C^*, y) = \frac{1}{\Delta t}\int_t^{t+\Delta t}\int_W^E\int_H^\eta \delta(C^* - C)vr\cos(y)\,dz\,dx\,dt, \tag{2}$$

where δ is the Dirac delta function, W and E are the eastern and western boundaries of the domain, H is the ocean bottom depth, η is the sea surface elevation, r is the radius of the earth, x is longitude, and t is time.

If the tracer (i.e., C) were density, the total transport within a layer bounded by ρ and $\rho + \Delta\rho$, could be determined from M_ρ^y by integrating from ρ to $\rho + \Delta\rho$. This is equivalent to averaging the transport within a layer of thickness h. The advantage of the distribution function approach of Pauluis et al. (2011) over the layer approach is that the quantity C needs not be monotonic in the vertical and C may be any passive or active scalar quantity. This approach was also taken by Nurser and Lee (2004), where the vertical transport is averaged in density coordinates at constant depth and the concept of discrete layers does not apply. A volumetric streamfunction in C versus latitude coordinates Ψ_{Cy} can be determined using

$$\Psi_{Cy}(C, y) = \int_{-\infty}^{C} M_C^y(C^*, y)\,dC^*. \tag{3}$$

As M is the volume transport per unit tracer, the meridional tracer transport T_C^y can be related to M via

$$\begin{aligned} T_C^y(y) &= \frac{1}{\Delta t}\int_t^{t+\Delta t}\int_W^E\int_H^\eta vCr\cos(y)\,dz\,dx\,dt \\ &= \int_{-\infty}^{+\infty} M_C^y(C, y)C\,dC, \end{aligned} \tag{4}$$

and considering $M_C^y(C, y) = d\Psi_{Cy}/dC$ and $\Psi_{Cy}(+/-\infty, y) = 0$, the chain rule can be applied to (4) to relate the tracer transport to the volumetric streamfunction

$$T_C^y(y) = \int_{-\infty}^{-\infty} \Psi_{Cy}(C, y)\,dC. \tag{5}$$

See Ferrari and Ferreira (2011) for an equivalent derivation of (5). A conceptual interpretation of (5) is that the tracer transport is proportional to the area under the Ψ_{Cy} curve. Ferrari and Ferreira (2011) use potential temperature θ as their scalar variable and can thus use $\Psi_{\theta y}$ to determine the meridional heat transport. Furthermore, Ferrari and Ferreira (2011) point out that a property transport can be determined for any range of C over which the net volume transport is zero, that is, a transport can be attributed to individual closed circulations. Put more precisely, given any two C values: C_i and C_j, such that $\Psi_{Cy}(C_i, y) - \Psi_{Cy}(C_j, y) = 0$, the flux of volume for all water between C_i and C_j is zero, by definition, and the flux of C because of that closed circulation is

$$\int_{C_i}^{C_j} [\Psi_{Cy}(C, y) - \Psi_{Cy}(C_i, y)]\,dC. \tag{6}$$

As such, Ferrari and Ferreira (2011) can decompose a given transport, in their case heat transport, into that because of various distinct circulation features.

Averaging transport only in terms of one tracer coordinate can alias circulations that are distinct in terms of another tracer coordinate. For example, water may flow in and out of a sea through a channel at the same density, but may be flowing in at a different temperature and salinity than when it is flowing out. Thus, a residual circulation in temperature or salinity may not be evident in density coordinates alone.

To capture the exchanges of multiple properties, joint distributions are used in two variable coordinates. In atmospheric literature, meridional transport has been averaged in dry entropy versus moist entropy coordinates (Pauluis et al. 2008; Laliberté et al. 2012). Such an analysis has revealed meridional exchanges of moisture within layers of constant entropy in a process dubbed moist recirculation (Laliberté et al. 2012). In oceanographic literature, transport across transcontinental sections has been averaged in potential temperature versus salinity coordinates (Cuny et al. 2002; Marsh et al. 2005). Such analysis has revealed exchanges not only of mass but also the concomitant exchanges of heat and salt (Fig. 1).

For any two variables C_1 and C_2, a two-scalar joint distribution $M_{C_1C_2}^y(C_1, C_2, y)$ may be defined such that

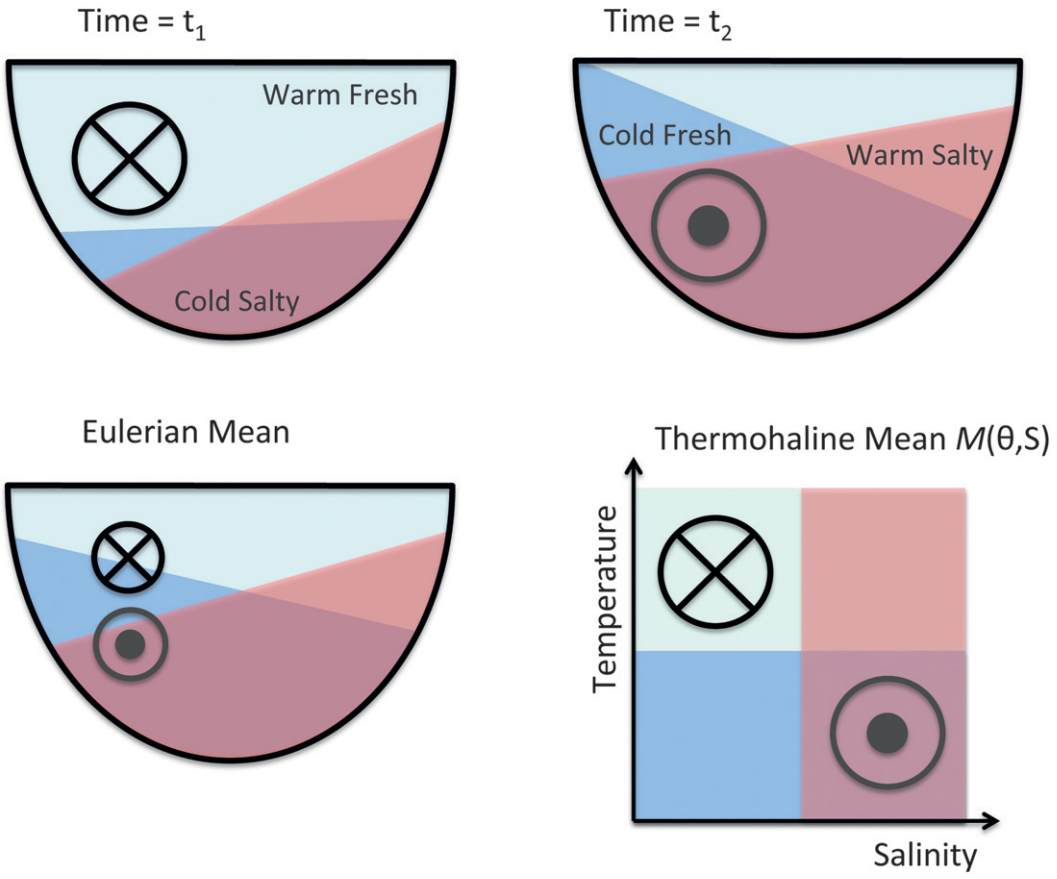

FIG. 1. Schematic describing the principle of thermohaline or two-scalar averaging. At time t_1, warm freshwater flows into the page. At time t_2, cold salty water flows out of the page. In the Eulerian mean, some of the flow at t_1 is cancelled by opposing flow at t_2. In the thermohaline mean, flow is averaged in temperature–salinity coordinates and the net transport of both heat and salt is preserved in the distribution function.

$$M^{y}_{C_1C_2}(C_1^*, C_2^*, y) = \frac{1}{\Delta t}\int_t^{t+\Delta t}\int_W^E\int_H^\eta \delta(C_1^* - C_1)\delta(C_2^* - C_2)vr\cos(y)\,dz\,dx\,dt. \tag{7}$$

The single-scalar distributions $M^{y}_{C_1}$ or $M^{y}_{C_2}$ can then be determined by summing $M^{y}_{C_1C_2}$ over all C_2 or all C_1, respectively.

Exchanges of heat and freshwater (FW) can occur both in the meridional and the vertical directions and averaging in one geographical coordinate may alias exchanges in another. To get a complete picture of the net diabatic circulation, it is instructive to average a geophysical flow in purely tracer coordinates:

$$\Psi_{C_1C_2}(C_1^*, C_2^*) = \frac{1}{\Delta t}\int_t^{t+\Delta t}\int_{C_1\le C_1^*|_{C_2^*}} \mathbf{u}\cdot\mathbf{n}_{C_2}\,dA\,dt \tag{8}$$

where $\mathbf{n}_{C_2}$ is the unit vector normal to surfaces of constant C_2 and $\int_{C_1\le C_1^*|_{C_2^*}} dA$ is the area integral above the surface where $C_2 = C_2^*$ and $C_1 \le C_1^*$. Note here that if a surface of constant C_2 is moving in time (i.e., the ocean is not steady) then $\Psi_{C_1C_2}$ represents both flow through a C_2 surface and the movement of that surface. A thermohaline streamfunction has been computed for a range of approximately steady ocean models and reveals a globally interconnected thermohaline circulation, otherwise aliased in geographical coordinates (Zika et al. 2012; Döös et al. 2012).

This study will draw on aspects of each of the studies mentioned above in the context of the vertical heat transport by ocean circulation. Like Pauluis et al. (2011), we take a statistical approach to averaging the transport. Following Ferrari and Ferreira (2011), we decompose the heat transport into contributions from various circulation features. By averaging in both temperature and salinity, we can further diagnose the energy conversion

and salt fluxes from each of those cells. We project each cell into geographical coordinates and then into purely thermohaline coordinates. Although the methods described in this study can generally be applied to any system with 1, 2, or indeed n scalar variables, we focus in particular on temperature and salinity as these are the two principal thermodynamic quantities carried by ocean models and from which other quantities such as density and pressure can be derived.

3. Model description

We use a version of the University of Victoria Earth System Climate Model, which is a climate model of intermediate complexity (UVic ESM; Weaver et al. 2001). The ocean component of UVic ESM is the Geophysical Fluid Dynamics Laboratory (GFDL) Modular Ocean Model, version 2.2 (MOM2.2; Pacanowski 1995), it employs a horizontal resolution of 1.8° latitude by 3.6° longitude, has 19 vertical levels, and is coupled to a 2D energy balance atmosphere. We use the same simulation as that described by Sijp et al. (2006), specifically their ''GM'' case [so named because it employs the eddy-induced advection parameterization of Gent and McWilliams (1990)] but with lower vertical mixing coefficients, increasing with depth, from a value of $0.3 \times 10^{-4}\,\mathrm{m^2\,s^{-1}}$ at the surface to $1.3 \times 10^{-4}\,\mathrm{m^2\,s^{-1}}$ at the bottom. UVic ESM employs the eddy-induced advection parameterization of Gent and McWilliams (1990) with a constant diffusion coefficient of $800\,\mathrm{m^2\,s^{-1}}$ and a flux-adjusted transport advection scheme (Gerdes et al. 1991). Tracers are diffused in the isopycnal direction with a constant coefficient of $1200\,\mathrm{m^2\,s^{-1}}$.

UVic ESM comprises an interactive single-layer energy balance atmospheric model with prescribed wind forcing. Wind forcing data from the National Centers for Atmospheric Prediction (NCEP)–National Center for Atmospheric Research (NCAR) reanalysis fields (Kalnay et al. 1996) are used, averaged over the period 1958–97 to form a seasonal cycle from the monthly fields.

The primary UVic ESM reference simulation analyzed here is integrated for 6000 years and achieves a statistically steady annual cycle by this time. Averages are formed from monthly mean velocity, potential temperature, and salinity fields over the final 10-yr period of the integration, comparisons between 5-day, monthly, and annually averaged diagnostics reveal qualitatively similar results (see the appendix). Variability is minimal at higher frequencies because of the low resolution of the model and the repeated wind forcing. Both the Eulerian velocity and the eddy-induced velocity [i.e., the transport due to the parameterization of Gent and McWilliams (1990)] are incorporated in all calculations of transport and transport streamfunctions. The heat transport diagnosed for these two terms is discussed in the appendix.

A further two experiments are analyzed here: TAU05 and TAU15, where the time-mean Southern Hemisphere westerly winds are reduced and increased by 50%, respectively. This is done by taking the standard NCEP wind field of the model and applying an amplification factor of 0.5 and 1.5 to the entire field, tapering it back to the original field outside the latitudes of the Southern Hemisphere westerlies [the locus where the zonally averaged zonal wind stress is positive in Fig. 1 of Sijp and England (2009)]. Note that we only consider the effect of a change in direct momentum transfer to the ocean associated with a change in wind magnitude. The wind change does not directly affect the model sea ice, evaporation, latent and sensible heat fluxes, etc. These only vary indirectly via changes in upper-ocean heat content and subsequent adjustment of the energy balance atmospheric model.

4. The thermal overturning circulation

To investigate the mechanisms by which the UVic ESM advects heat vertically, we compute a distribution function M_θ^z for the vertical volume transport in potential temperature coordinates

$$M_\theta^z(\theta^*,z)=\frac{1}{\Delta t}\int_t^{t+\Delta t}\int_{-180^\circ}^{180^\circ}\int_{-90^\circ}^{90^\circ}\delta(\theta^*-\theta)wr^2\cos(y)\,dx\,dy\,dt, \tag{9}$$

where x is the longitudinal coordinate, y the latitudinal coordinate, z the vertical coordinate, δ is the Dirac delta function, w is the vertical velocity (note that we use w to signify the sum of the Eulerian and parameterized eddy transport velocity), and r is the radius of the earth (here assumed spherical). At some depth z, $M_\theta^z(\theta^*, z)$ can be interpreted as the area integral of the vertical velocity where $\theta = \theta^*$. In practice, $M_\theta^z(\theta^*, z)$ is computed as a histogram with bin intervals of 0.1°C. We show in the appendix that this is sufficiently accurate for our purposes.

The thermal overturning streamfunction (a streamfunction in temperature–depth coordinates) may thus be determined from M_θ^z using

$$\Psi_{\theta z}(\theta,z)=\int_{-\infty}^{\theta}M_\theta^z(\theta^*,z)\,d\theta^*. \tag{10}$$

The thermal overturning streamfunction is shown in Fig. 2. Components of the streamfunction that rotate anticlockwise transport cooler water downward and warmer water upward and are thermally direct. Components that rotate clockwise transport warmer water downward and colder water upward and are thermally indirect. The streamfunction contains three dominant

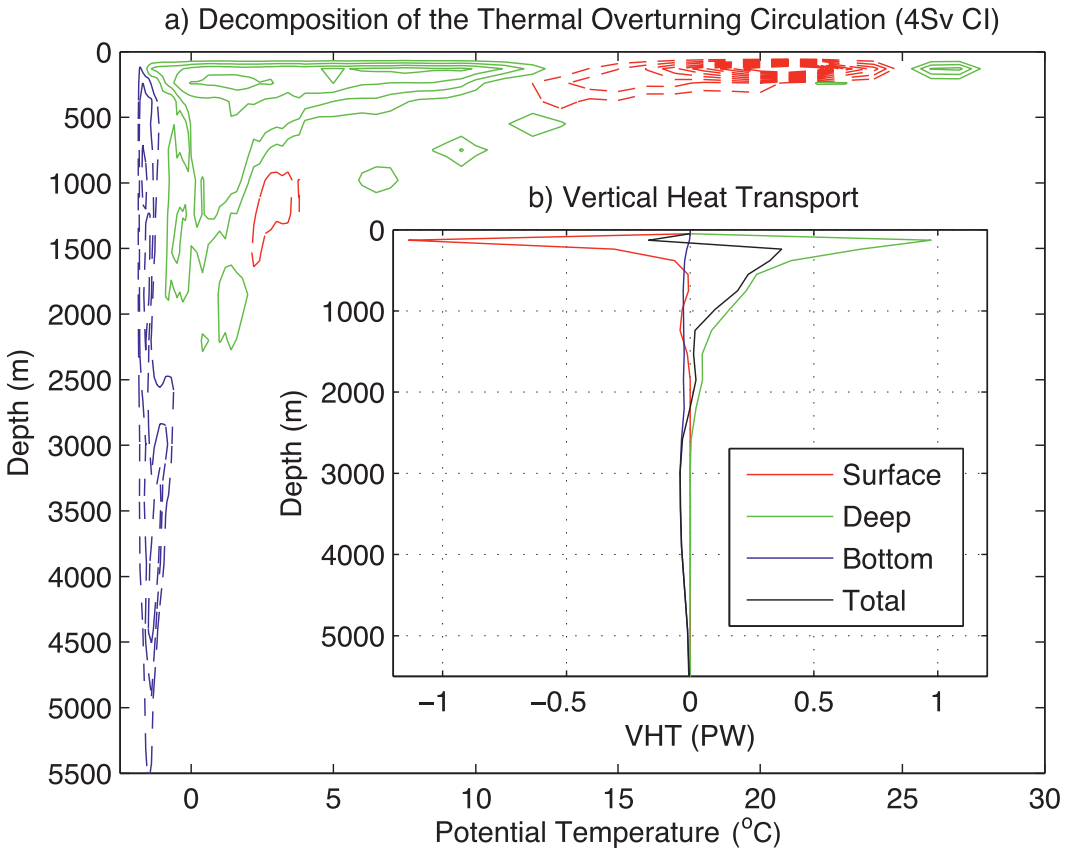

FIG. 2. (a) The thermal overturning streamfunction $\Psi_{\theta z}$. Dashed lines are anticlockwise and solid lines are clockwise; contour interval (CI) = 4 Sv. Anticlockwise cells in temperature coordinates flux heat upward and are separated into a deep (blue; $\theta < 1°C$) and surface (red; $\theta > 1°C$) cell. The remaining clockwise cell (green) fluxes heat downward. (b) Downward advective vertical heat transport (PW; PW = 10^{15} W) due to each of the cells shown in (a).

cells: a thermally direct bottom cell between −2° and −1°C, extending to below 5500 m (blue in Fig. 2); a thermally indirect deep cell between −1° and 15°C, extending down to 2000 m (green in Fig. 2); and a thermally direct surface cell between 10° and 25°C, occupying the upper 500 m (red in Fig. 2). For the remainder of this study, we define the bottom cell to be all negative streamfunction values colder than 1°C, the deep cell simply as all positive streamfunction values, and the shallow cell to be the remaining negative values warmer than 1°C. Choosing other temperatures between 1° and 8°C yields the same qualitative results.

As we have averaged the transport in temperature coordinates, we are able to calculate the vertical heat transport T_H^z. From (5),

$$T_H^z(z) = \int_{-\infty}^{+\infty} \rho_0 C_p \Psi_{\theta z}\, d\theta, \tag{11}$$

where ρ_0 is a reference density (taken here to be 1025 kg m^{-2}), and C_p is the heat capacity of seawater (taken here to be 4000 J K^{-1}). Because the model discussed here conserves potential temperature exactly, all heat transport calculations are made using this quantity. In calculations based on observations, the appropriate heat variable to use is conservative temperature (McDougall 2003).

The bottom, deep, and surface cells are distinct in temperature–depth coordinates. Thus, following Ferrari and Ferreira (2011), we can separate the heat transport contribution due to each cell by integrating separately over the temperature ranges they occupy, namely

$$T_{H-\mathrm{Bottom}}^z(z) = \int_{-\infty}^{1^\circ} \rho_0 C_p \Pi(-\Psi_{\theta z}) \Psi_{\theta z}(\theta, z)\, d\theta, \tag{12}$$

$$T^z_{H-\mathrm{Deep}}(z) = \int_{-\infty}^{+\infty} \rho_0 C_p \Pi(\Psi_{\theta z}) \Psi_{\theta z}(\theta, z)\, d\theta, \quad \text{and} \tag{13}$$

$$T^z_{H-\mathrm{Surface}}(z) = \int_{1^\circ}^{+\infty} \rho_0 C_p \Pi(-\Psi_{\theta z}) \Psi_{\theta z}(\theta, z)\, d\theta, \tag{14}$$

where Π is the unit step function [$\Pi(x) = 1$ for $x > 0$ and $\Pi(x) = 0$ otherwise]. The total vertical heat transport and that due to each of the thermal cells is shown in Fig. 2b. As both Gnanadesikan et al. (2005) and Gregory (2000) observed, the advective vertical heat transport between 200 and 2000 m is downward. In UVic ESM, the vertical heat transport peaks at 0.4 PW around 200 m. This net downward heat flux is due to the dominance of the deep cell that peaks close to 1 PW and is compensated by the surface-intensified surface and the bottom cells.

In summary, we have isolated the three dominant cells that contribute to the vertical heat flux in the ocean model. We now seek to determine how these three cells relate to the various cells of the meridional overturning circulation.

5. Geographical distribution of vertical heat transport

We are interested in the geographical distribution of the bottom, deep, and surface thermal cells discussed in the previous section. To isolate the latitude at which up- and downwelling occurs within each cell, we average the vertical volume transport in both temperature and latitude coordinates using the joint distribution

$$M^z_{\theta y}(\theta, y, z) = \frac{1}{\Delta t} \int_t^{t+\Delta t} \int_{-180^\circ}^{180^\circ} \delta(\theta^* - \theta)\delta(y^* - y) w\, dx\, dt. \tag{15}$$

The joint distribution $M^z_{\theta y}$ is shown in Fig. 3a for the 550-m-depth level. An accumulative integral of $M^z_{\theta y}$ from the coldest to warmest waters reveals the streamfunction $\Psi_{\theta z}$ described in the previous section (Fig. 3b). Alternatively, $M^z_{\theta y}$ can be cumulatively integrated in the y direction to reveal the conventional meridional overturning streamfunction Ψ_{yz} (the black line in Fig. 3c shows the value of the streamfunction at constant depth).

Using $\Psi_{\theta z}$, closed cells are identified where the total vertical volume transport is zero. The deep cell for example is closed between $\theta = -1^\circ$ and 11°C at 550 m (green region in Figs. 3a,b). In computing $M^z_{\theta y}$, the vertical transport is averaged in both temperature and latitude coordinates. Integrating $M^z_{\theta y}$ accumulatively with latitude and between $\theta = -1^\circ$ and 11°C, a streamfunction is defined describing the latitudes at which up- and downwelling occur within the deep cell. More generally

$$\Psi^{\mathrm{Deep}}_{yz}(y, z) = \int_{-90^\circ}^{y} \int_{-\infty}^{+\infty} \Pi(\Psi_{\theta z}) M^z_{\theta y}(\theta, y^*, z) r^2 \cos(y^*)\, d\theta\, dy^*. \tag{16}$$

The meridional streamfunction is effectively computed in (16), masking out all water masses associated with the bottom and surface cells. Thus, the meridional overturning streamfunction $\Psi^{\mathrm{Deep}}_{yz}$ only describes the up- and downwelling that occurs within the deep cell.

The bottom and surface cells of the thermal overturning circulation are delineated by being thermally direct ($\Psi_{\theta z} > 0$), with the bottom cell occupying $\theta < 1^\circ$ and the surface cell $\theta \geq 1$°C. Thus, the two cells can be projected into depth–latitude coordinates using

$$\Psi^{\mathrm{Bottom}}_{yz}(y, z) = \int_{-90^\circ}^{y} \int_{-\infty}^{1^\circ} \Pi(-\Psi_{\theta z}) M^z_{\theta y}(\theta, y^*, z) r^2 \cos(y^*)\, d\theta\, dy^* \quad \text{and} \tag{17}$$

$$\Psi^{\mathrm{Surface}}_{yz}(y, z) = \int_{-90^\circ}^{y} \int_{1^\circ}^{+\infty} \Pi(-\Psi_{\theta z}) M^z_{\theta y}(\theta, y^*, z) r^2 \cos(y^*)\, d\theta\, dy^*. \tag{18}$$

Note above, that the Π function masks out water masses within the clockwise (thermally indirect) cell leaving only the anticlockwise (thermally direct) parts of the streamfunction, while the θ limits on the integral are used to distinguish between the cold bottom and warm surface, components.

The resulting decomposition of the depth–latitude overturning is shown in Fig. 4. The bottom cell constitutes the Antarctic Bottom Water circulation. The deep cell encompasses both the Southern Ocean overturning circulation, the Atlantic meridional overturning circulation, and the Antarctic Intermediate Water circulation in the Pacific. Finally, the surface cells encompass the subtropical gyre circulations and the shallow overturning cells in the tropics and subtropics.

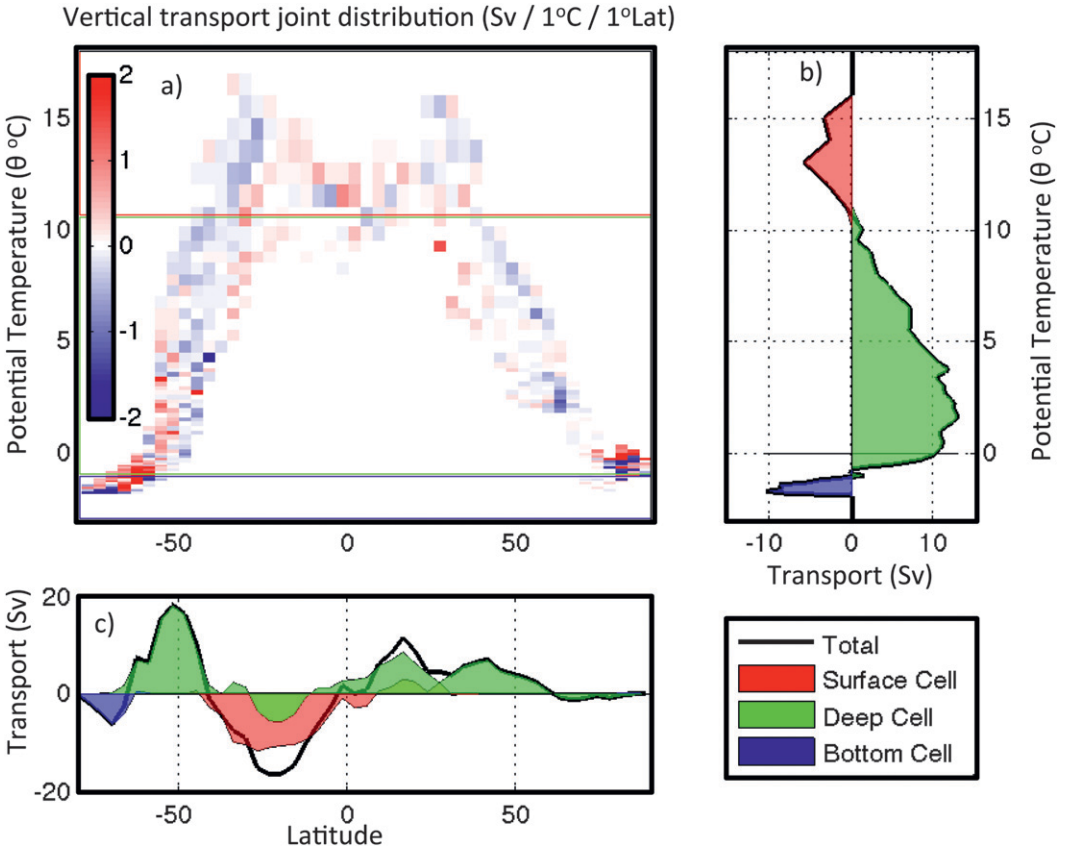

FIG. 3. (a) Joint distribution of vertical transport in temperature–latitude coordinates at 550-m depth. Negative (blue) represents net downward motion and positive (red) represents upward motion. The blue box shows the range of temperature values where a closed bottom cell in temperature coordinates exists, the green box shows the range for the deep cell, and the red box shows the range for the surface cell. (b) Accumulated volume transport [$\Psi_{\theta z}(\theta, z = 550\,\text{m})$] in temperature coordinates for the bottom, deep, and surface cells each summing to give zero volume transport. (c) Accumulated vertical transport through the 550-m-depth surface as a function of latitude [$\Psi_{yz}(y, z = 550\,\text{m})$] for the bottom, deep, and surface cells diagnosed by integrating the transport in the blue, green, and red boxes of (a), respectively. Negative latitudes are south of the equator.

6. Vertical salt and buoyancy transport by the thermal cells

We are now interested in the physical mechanisms by which the various thermal cells, identified previously, achieve their vertical heat transport. To do this, we will determine the density at which water up- and downwells and, thus, whether circulation can be driven by buoyant processes or whether mechanical forcing is required to induce circulation.

According the equation of state of seawater (McDougall 2003), density is a function of temperature, salinity, and pressure. Pressure is a strong function of depth. Hence, the density at which water up- and downwells at a particular depth depends on its temperature and salinity. Thus, we thus compute the joint distribution of vertical volume transport in temperature and salinity coordinates $M^z_{\theta S}$ defined by

$$M^z_{\theta S}(\theta, S, z) = \frac{1}{\Delta t}\int_t^{t+\Delta t}\int_{-180^\circ}^{180^\circ}\int_{-90^\circ}^{90^\circ}\delta(\theta^* - \theta)\delta(S^* - S)wr^2\cos(y)\,dy\,dx\,dt. \quad (19)$$

Here, $M^z_{\theta S}(\theta^*, S^*, z)$ can be interpreted as the integral of the vertical velocity, where $\theta = \theta^*$ and $S = S^*$. The salinity interval used when determining salt and buoyancy fluxes is $0.05\,\text{g}\,\text{kg}^{-1}$.

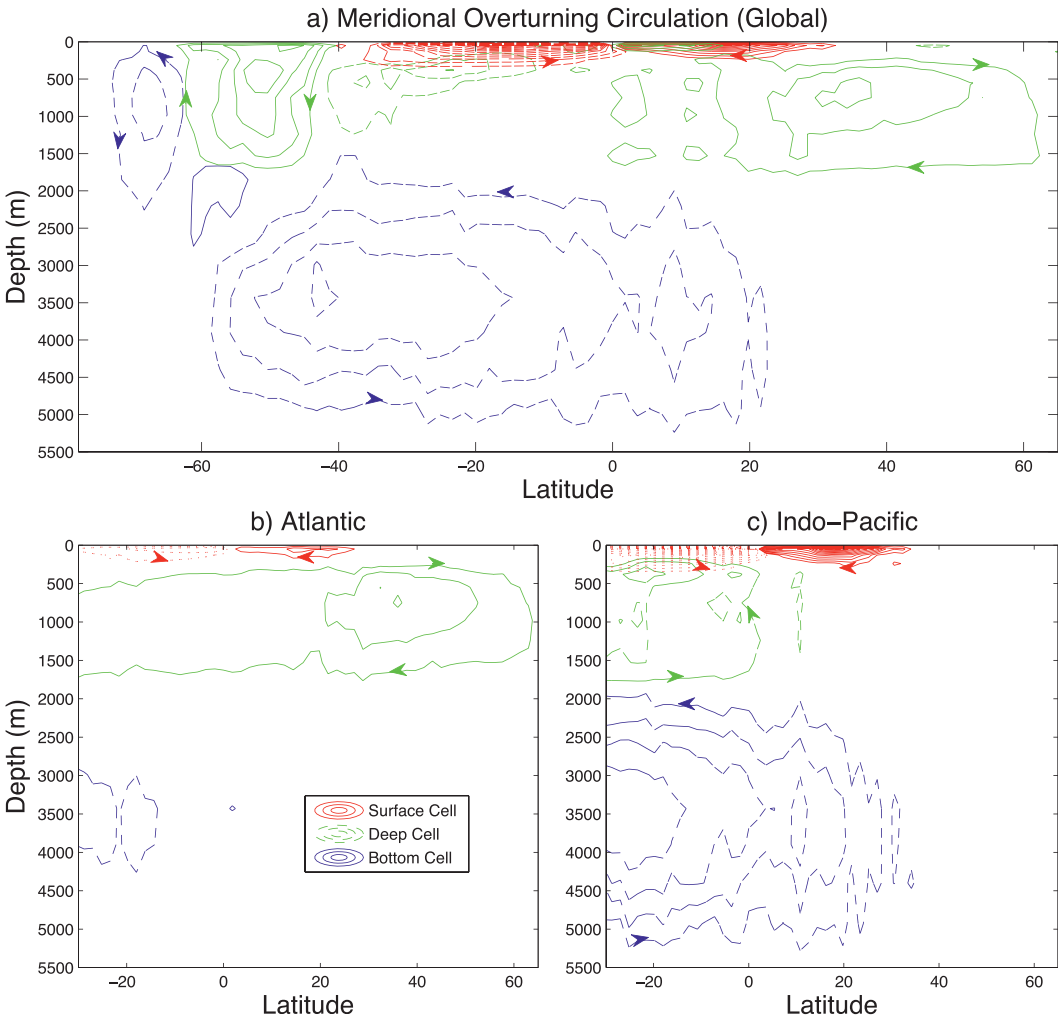

FIG. 4. Surface, deep, and bottom cells projected into depth–latitude coordinates. Solid cells are anticlockwise and dashed cells are clockwise; CI = 4 Sv. The sum of all three circulations is the meridional overturning streamfunction. Negative latitudes are south of the equator.

The thermohaline joint distribution of vertical advection at 550 m reveals many distinct water mass exchanges (Fig. 5a). The coldest sinking water ($S \approx 34.8\,\mathrm{g\,kg^{-1}}$ and $\theta < 0$°C) is AABW. Flowing upward within $34.8 < S < 35.2\,\mathrm{g\,kg^{-1}}$ and $-1° < \theta < 4$°C is Circumpolar Deep Water (CDW). Other sinking water includes North Atlantic Deep Water (NADW; $S > 34.7\,\mathrm{g\,kg^{-1}}$ and $2° < \theta < 5$°C) and Intermediate Water ($S < 34.7\,\mathrm{g\,kg^{-1}}$ and $3° < \theta < 10$°C). The remaining water warmer than 10°C forms a variety of mode and thermocline waters.

As in the previous section where cells distinct in temperature–depth coordinates were projected into depth–latitude coordinates, here these cells are projected into depth–salinity coordinates. The streamfunction in depth–salinity coordinates (the haline overturning streamfunction), representative only of the deep cell is

$$\Psi_{Sz}^{\mathrm{Deep}}(S,z) = \int_{-\infty}^{S}\int_{-\infty}^{+\infty} \Pi(\Psi_{\theta z}) M_{\theta S}^{z}(\theta, S^{*}, z)\, d\theta\, dS^{*}. \tag{20}$$

The haline overturning streamfunctions for the bottom $\Psi_{Sz}^{\mathrm{Bottom}}$ and surface $\Psi_{Sz}^{\mathrm{Surface}}(S, z)$ cells are defined by analogy with (17) and (18), respectively.

The bottom cell, when projected into saline coordinates, fluxes saline water downward and fresher water upward (Fig. 6a). This is consistent with the formation of extremely dense Antarctic Bottom Water through both cooling and brine rejection at the Antarctic margins, which warms and freshens as it sinks into the deep ocean. The surface cell also advects salt downward, consistent with higher-salinity water being pumped downward in the center of the subtropical gyres. The deep cell is made up

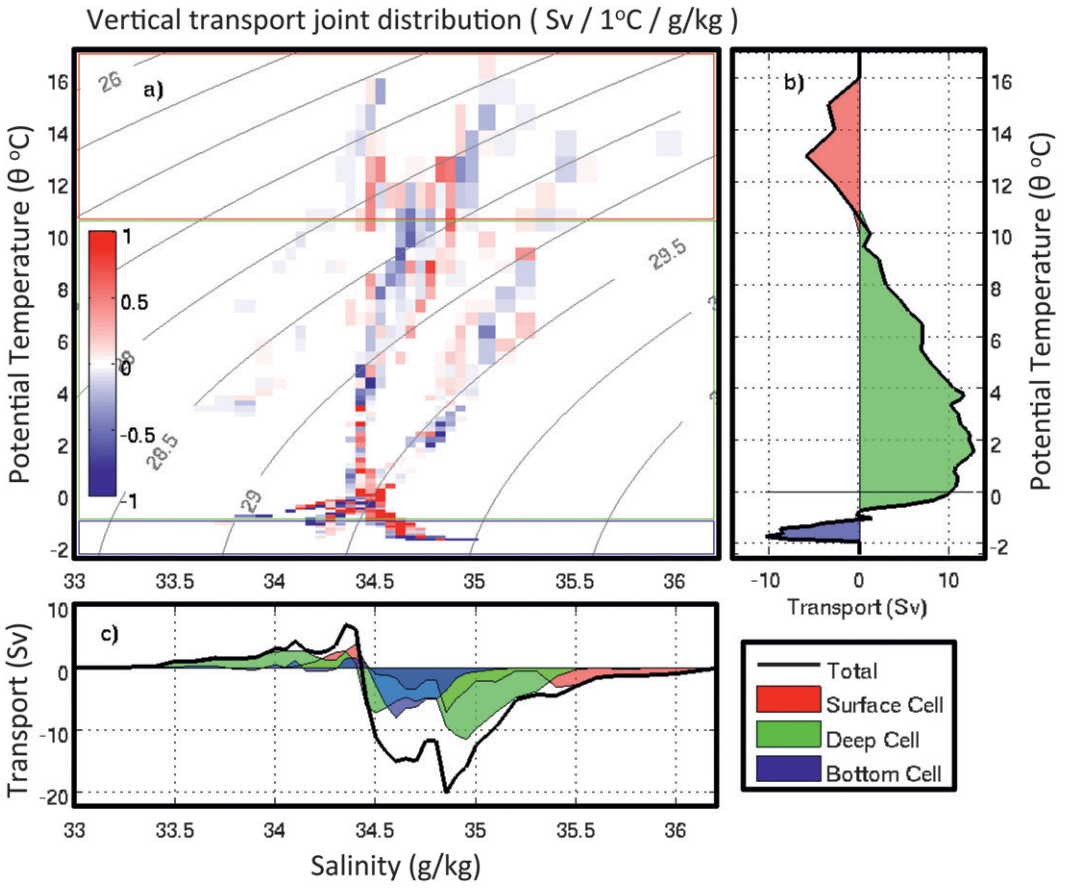

FIG. 5. (a) As in Fig. 3a, but for temperature–salinity coordinates. (b) Accumulated volume transport [$\Psi_{\theta z}$ (θ, z = 550 m)] in temperature coordinates for the bottom, deep, and surface cells each summing to give zero volume transport. (c) As in Fig. 3c, but for salinity coordinates [Ψ_{Sz} (S, z = 550 m)].

of two subcells—one larger saline subcell that advects salt downward between the surface and 2500-m depth, and a smaller subsurface fresh subcell that advects the freshest water downward only between 500- and 2000-m depth. Additional analysis projecting these subcells into geographical coordinates (not shown) has found that the saline subcell is related to the NADW branch of the overturning that involves more saline water sinking, while the fresh subcell is related to the Southern Ocean circulation where relatively fresh intermediate water is pumped downward. Despite the fresh subcell, the deep cell upwells lower-salinity water and downwells higher-salinity water throughout the majority of the water column.

As was done with vertical heat transport, we compute the vertical freshwater transport T^z_{FW} resulting from each cell given the saline streamfunction Ψ_{Sz}. The salt flux for the deep cell is, for example,

$$T^z_{\mathrm{FW-Deep}}(z) = -\frac{1}{S_0}\int_{-\infty}^{+\infty} \Psi^{\mathrm{Deep}}_{Sz}\, dS. \qquad (21)$$

Above, the total transport of salt by the deep cell is converted into a freshwater transport T^z_{FW} by dividing by a reference salinity S_0 (here, we take $S_0 = 35\,\mathrm{g\,kg^{-1}}$).

The total advective freshwater transport in the model is always upward (Fig. 6b), meaning that salt is advected downward by the resolved circulation of the model and transported upward by mixing and other subgrid-scale processes. All three cells flux salt downward through most of the water column. However, the deep cell fluxes a small amount of salinity upward around 1500-m depth where an anticlockwise cell in S–z coordinates dominates. Although we do not discuss the full freshwater budget here, in this simulation, the steady upward transport of freshwater by circulation is in addition to an upward flux of freshwater by isopycnal and convective mixing. These three terms are balanced by a downward flux of freshwater by stratified vertical mixing.

In this model, salinity makes the downwelling branch of the deep cell denser and the upwelling branch of the deep cell lighter in the upper 1000 m. We now investigate the combined effect of heat and salt on the buoyancy

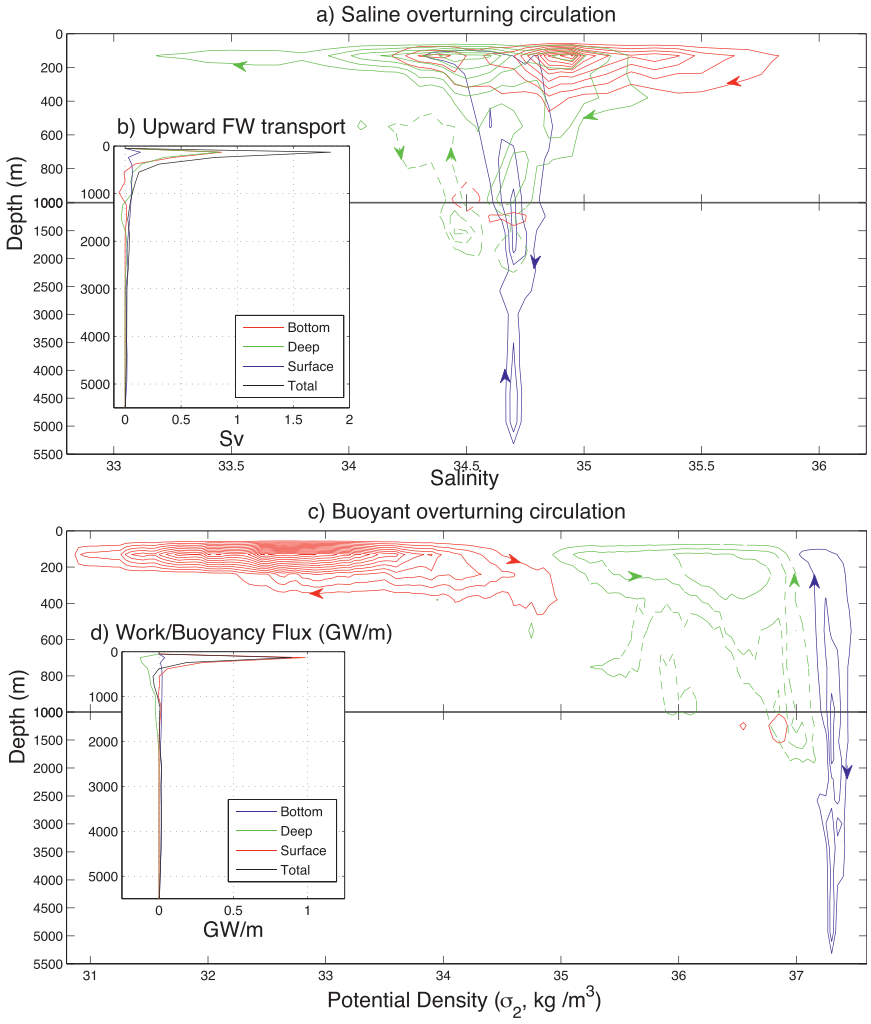

FIG. 6. (a) Decomposition of the depth–salinity streamfunction into a bottom (blue), deep (green), and surface (red) cell each of which is distinct in temperature–depth coordinates. Dashed lines are anticlockwise and solid lines are clockwise; CI = 4 Sv. Clockwise cells flux salt downward and freshwater upward. (b) Upward vertical freshwater transport (Sv) for each of the cells shown in (a). (c) As in (a), but for a decomposition of the potential depth–density streamfunction. (d) Conversion rate of available potential energy per vertical meter, proportional to the vertical buoyancy transport ($\mathrm{GW\,m^{-1}}$). Energy conversion rates in (d) are computed using in situ density rather than σ_2.

transport and hence the energy conversion by the three cells. As Nycander et al. (2007) point out, it is insightful to compute an overturning streamfunction in depth–density coordinates. Any overturning cell in depth–density coordinates implies a vertical flux of buoyancy. In addition, a vertical flux of buoyancy implies a conversion from available potential energy to mechanical energy or vice versa.

The overturning streamfunction in depth–density coordinates $\Psi_{\rho z}$ can be determined from $M^z_{\theta S}$ using

$$\Psi_{\rho z}(\rho^*, z) = \int_{-\infty}^{+\infty}\int_{-\infty}^{+\infty} \Pi[\rho^* - \rho(\theta, S, z)] M^z_{\theta S}(\theta, S, z)\, d\theta\, dS. \tag{22}$$

The streamfunction for each cell is computed as in (20) by integrating only over those θ values that each cell occupies.

The vertical buoyancy transport T^z_b is then

$$T^z_b(z) = -g\int_{-\infty}^{+\infty} \Psi_{\rho z}\, d\rho. \tag{23}$$

The vertical buoyancy transport is related to the conversion from available potential energy to kinetic energy (Nycander et al. 2007) via

$$W = \int_H^0 T^z_b(z)\, dz. \tag{24}$$

The vertical buoyancy transport T_b^z can be interpreted as a work per unit depth ($\mathrm{GW\,m^{-1}}$; where $1\,\mathrm{GW} = 10^9\,\mathrm{W}$). Upward vertical buoyancy transport decreases the potential energy of the system, while downward buoyancy transport increases the potential energy. For illustrative purposes, we map the bottom, deep, and surface cells into potential density referenced to 2000-m depth σ_2; however, when we calculate the vertical buoyancy transport, we use in situ density (Figs. 6c,d).

The bottom and surface cells flux dense water downward and light water upward. Both cells are thermally direct implying they convert available potential energy to mechanical energy. The deep cell fluxes light water downward and dense water upward thus converting mechanical energy into potential energy. The deep cell must be mechanically forced, as buoyancy-driven processes cannot lift light water upward.

The surface cell energy conversion rate peaks at $1\,\mathrm{GW\,m^{-1}}$ around 100–200-m depth (the base of the mixed layer through which near-surface mixing and radiative heat fluxes penetrate). The bottom cell converts available potential energy into kinetic energy throughout the water column at around $0.02\,\mathrm{GW\,m^{-1}}$. The deep cell converts up to $0.12\,\mathrm{GW\,m^{-1}}$ of kinetic energy to available potential energy at 200-m depth, decaying to zero at around 2000-m depth.

7. A decomposition of the thermohaline circulation

We now wish to understand the way in which the thermally indirect deep cell gains salinity at the surface, making the sinking branch denser than it would otherwise be and reducing the mechanical energy needed to maintain it. More broadly, this can be seen as asking the role of the deep cell (which we have already shown to be associated with the upper branch of the meridional overturning circulation) in the interconnected thermohaline circulation. Here, we define thermohaline circulation as the integrated transport in purely thermohaline coordinates (Zika et al. 2012; Döös et al. 2012).

Just as the transport across a depth surface was averaged in temperature and salinity coordinates to yield the joint distribution $M_{\theta S}^z$, we can diagnose a joint distribution across any isosurface in terms of any number of scalar quantities. We now average the transport of UVic ESM across isotherms in depth and salinity coordinates

$$M_{zS}^{\theta}(\theta, S, z) = \frac{1}{\Delta t}\int_t^{t+\Delta t}\int_{\theta}\delta(z - z^*)\delta(S - S^*)\mathbf{u}\cdot\mathbf{n}_{\theta}\,dA\,dt, \tag{25}$$

where $\int_{\theta} dA$ is the integral over the surface of constant temperature θ, and $\mathbf{u}\cdot\mathbf{n}_{\theta}$ is the absolute velocity normal to the temperature surface. Note that if the isotherm is moving in space throughout the averaging period, then $\mathbf{u}\cdot\mathbf{n}_{\theta}$ represents movement of an isotherm in addition to water mass transformation. In the model discussed here, the isotherms are approximately steady over the 10-yr-averaging period. From M_{zS}^{θ}, the thermohaline streamfunction $\Psi_{\theta S}$ can be derived using

$$\Psi_{\theta S}(\theta, S) = \int_0^H\int_{-\infty}^S M_{zS}^{\theta}(\theta, S^*, z)\,dS^*\,dz, \tag{26}$$

where the ocean surface is considered to be at $z = 0$ and the bottom at $z = H$. As an alternative to (26), the temperature–depth overturning can be diagnosed from M_{zS}^{θ} using

$$\Psi_{\theta z}(\theta, z) = \int_0^z\int_{-\infty}^{+\infty} M_{zS}^{\theta}(\theta, S, z^*)\,dS\,dz^*. \tag{27}$$

The advantage of having averaged in depth and temperature coordinates is that the cells that are distinct in temperature–depth coordinates from the previous sections, namely the bottom, deep, and surface cells, can be projected into temperature–salinity coordinates using

$$\Psi_{\theta S}^{\mathrm{Bottom}}(\theta, S) = \int_0^H\int_{-\infty}^S \Pi[-\Psi_{\theta z}(\theta, z)]\Pi(\theta - 1^\circ)M_{zS}^{\theta}(\theta, S^*, z)\,dS^*\,dz, \tag{28}$$

$$\Psi_{\theta S}^{\mathrm{Deep}}(\theta, S) = \int_0^H\int_{-\infty}^S \Pi[\Psi_{\theta z}(\theta, z)]M_{zS}^{\theta}(\theta, S^*, z)\,dS^*\,dz, \quad \text{and} \tag{29}$$

$$\Psi_{\theta S}^{\mathrm{Surface}}(\theta, S) = \int_0^H\int_{-\infty}^S \Pi[-\Psi_{\theta z}(\theta, z)]\Pi(1^\circ - \theta)M_{zS}^{\theta}(\theta, S^*, z)\,dS^*\,dz. \tag{30}$$

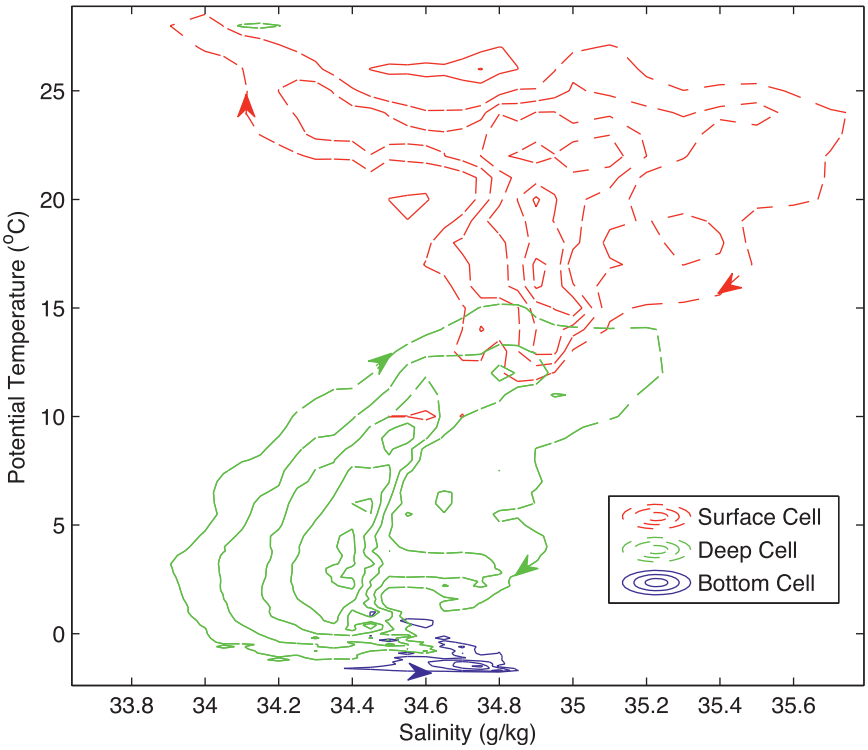

FIG. 7. Surface, deep, and bottom cells, projected into temperature–salinity coordinates. Solid cells are anticlockwise and dashed cells are clockwise; CI = 4 Sv.

In purely thermohaline coordinates, the deep and surface cells are both clockwise (Fig. 7). The two cells make up what was described by Zika et al. (2012) and Döös et al. (2012) as the global cell of the thermohaline circulation. The deep cell encompasses the cooling of high-salinity Atlantic water to form North Atlantic Deep Water around 35 g kg^{-1} and 5°C. This water ultimately freshens and cools forming Antarctic Surface and Intermediate Waters near 2°C. These waters then warm and reach a junction with the waters of the surface cell within $12° < \theta < 15$°C. The freshest waters within this temperature range are warmed within the surface cell to form water masses of the tropics and subtropics (around 25°C). At high temperatures, these waters become more saline through low-latitude evaporation. Within the surface cell, waters are then cooled, reentering the temperature ranges where the deep and surface cells overlap at a higher salinity than when they exited.

Although the surface and deep circulations are not connected in temperature–depth coordinates (Fig. 2) nor in depth–latitude coordinates (Fig. 4), their projection into thermohaline coordinates demonstrates that the two circulation features transit through the same water masses and are thus likely to form one interconnected circulation. A significant fraction (approximately 16 Sv; where 1 Sv $\equiv 10^6$ m^3 s^{-1}) of the surface cell apparently becomes more fresh, migrating from $S = 35$ to 34.5 g kg^{-1} between $\theta = 12°$ and 15°C. The surface cell is, in fact, beneath the deep cell at these temperatures (Fig. 2). Thus, this freshening cannot be caused by direct forcing from the sea surface and must occur as a result of mixing with relatively freshwater (most likely within the deep cell) or through the exchange at constant depth of lower-salinity waters with the deep cell (an exchange that would be masked out in temperature–depth coordinates). So, it is likely that there is either an exchange of saline water from the surface to the deep cell and an exchange of freshwater from the deep to the surface cell either through an explicit advective exchange or through subgrid-scale mixing processes.

To summarize, we have shown that the salinity gain within the deep cell occurs where the deep and surface gyre circulations interact, suggesting the high salinities achieved within the sinking branch are coupled to evaporative processes in the subtropics. Saline effects, in some models, may lead to the sinking branch of the deep cell being denser than the upwelling branch, allowing the deep cell to flux heat downward without the need for mechanical forcing. However, in the model discussed here, the deep cell requires mechanical forcing to be maintained. In the next section, we discuss the sensitivity of the deep cell to changes in the magnitude of that mechanical forcing.

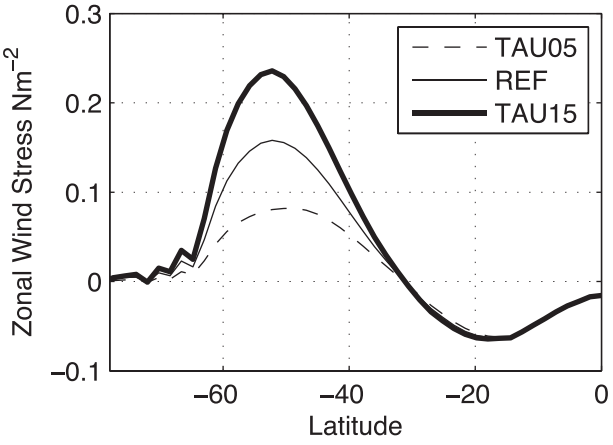

FIG. 8. Zonally averaged wind stress for the wind perturbation experiments: TAU05, reference (REF), and TAU15. Negative latitudes are south of the equator.

8. The role of wind forcing

In section 6, it was shown that the thermally direct deep cell fluxes light water downward and dense water upward. Such a circulation requires mechanical forcing to be sustained (Nycander et al. 2007) and this forcing may come from Southern Hemisphere winds (Toggweiler and Samuels 1995). To confirm that there is a relationship between the deep cell's strength and the mechanical forcing provided by the Southern Hemisphere winds, we carry out two wind perturbation experiments, wherein the zonal and meridional components of wind stress south of 30°S are multiplied by factors of 0.5 and 1.5, respectively (experiments TAU05 and TAU15; Fig. 8).

Although the experiments described involve large wind stress perturbations, considering past and predicted future climates, they allow us to better understand the fundamental role of wind forcing in driving ocean circulation and vertical heat fluxes in the model. In addition, the mechanisms by which the wind-forced circulation is countered in the Southern Ocean is only crudely parameterized in our model. Hence, a lower wind stress experiment, for example, could also be thought of as an ocean state with higher eddy compensation for the wind-driven circulation.

Here, we diagnose the thermal overturning streamfunction for TAU05 and TAU15 and undertake the same decomposition into a bottom, deep, and surface cell as in section 4 (Fig. 9). With weaker winds, the thermally indirect deep cell occupies only the surface layers and is weaker than in the reference experiment with a transport of only 20 Sv (Fig. 9a). Furthermore, the thermally direct surface cell occupies the temperatures previously occupied by the deep cell between 500 and 1500 m with a strength of 10 Sv. By projecting the surface and deep cells of TAU05 into depth–latitude coordinates, we find that a significant portion of the upper limb of the meridional overturning is occupied by the surface cell (not shown). This suggests that, with weaker Southern

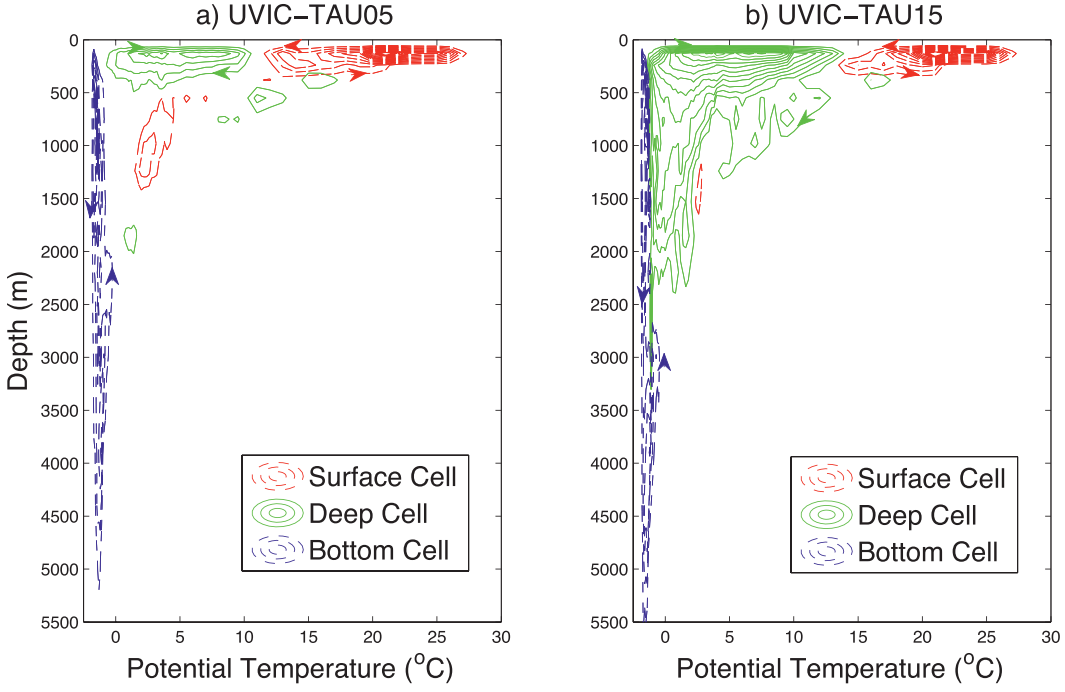

FIG. 9. Thermal overturning streamfunction (CI = 4 Sv) decomposed into a bottom, deep, and surface cell as in Fig. 2 for (a) TAU05 and (b) TAU15. Solid cells are counterclockwise and dashed cells are clockwise.

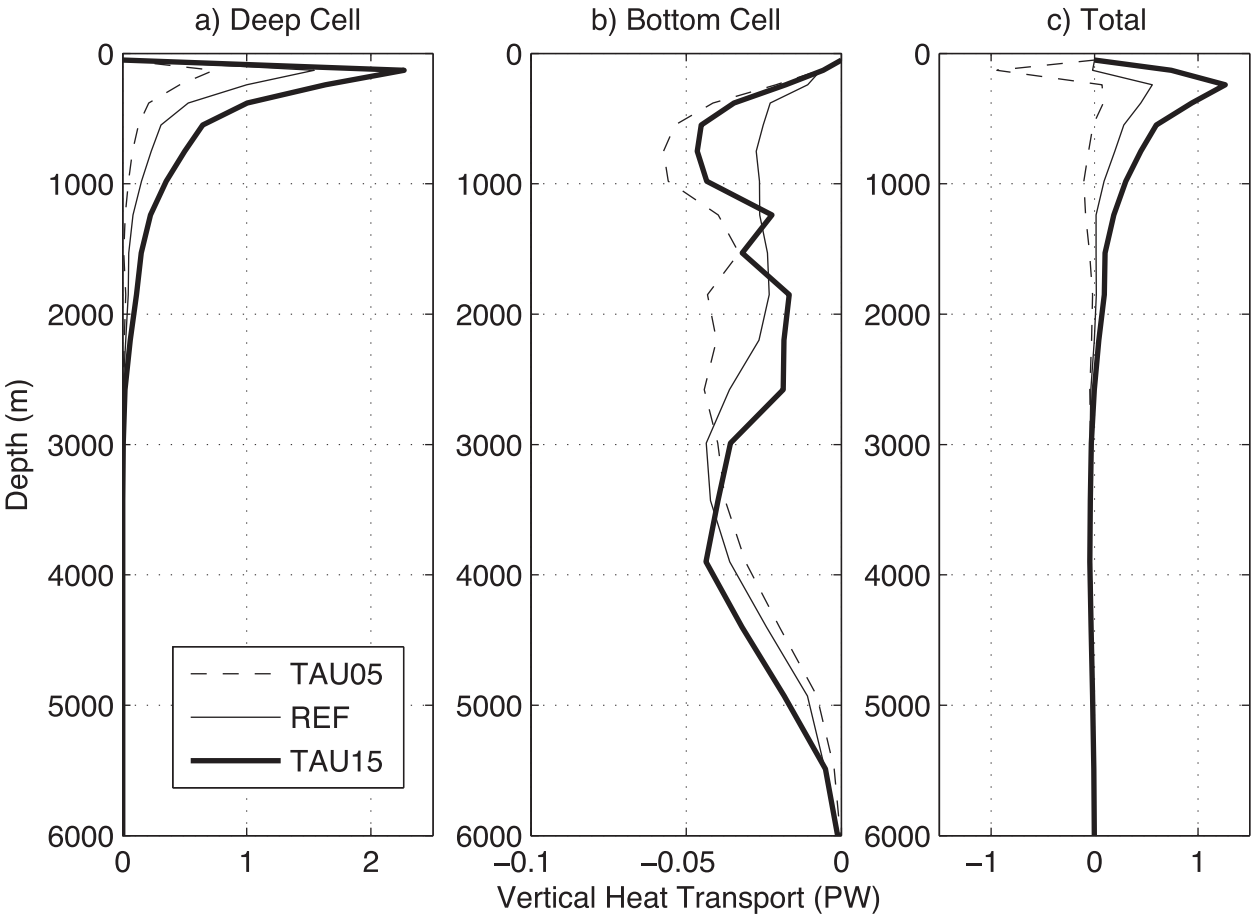

FIG. 10. Vertical advective heat transport (PW) for experiments TAU05 (dashed), REF (thin solid), and TAU15 (thick) for (a) the deep overturning cell, (b) the bottom cell, and (c) the total circulation.

Hemisphere winds (or with greater eddy compensation and/or a stronger thermally direct circulation in the North Atlantic), the upper limb of the overturning circulation could indeed be net thermally direct. In contrast, both the bottom and surface cells (aside from the cell lying below the deep cell) retain their approximate strength and structure under reduced Southern Hemisphere winds (Fig. 9a).

With increased winds, the deep cell increases in strength to 15 Sv. The deep cell occupies approximately the same temperature ranges and depths but is more vigorous throughout. Below 3000-m depth, the bottom cell is noticeably strengthened and deepened with the −4 Sv contour extending now below 5500 m, suggesting some coupling between the deep and bottom cells in this model. The surface cell remains approximately the same as in the reference experiment.

We now compute the heat transport from total circulation and from the bottom and deep thermal cells following the same procedure as described in section 4 (Fig. 10). Maximum heat transports are 0.75, 1.55, and 2.25 PW for experiments TAU05, REF, and TAU15, respectively (Fig. 10a). This suggests a nearly linear relationship between the heat transported by the deep cell and the wind forcing. The apparent linear relationship holds for the entire profile of the heat transport down to 2000-m depth. The linear relationship between the mechanical forcing by the winds and the deep cell is consistent with the energetic analysis presented in section 6.

Heat transport by the bottom cell in the upper 3000 m of the ocean does not respond to changed winds in a coherent way (Fig. 10b). However, in the deep ocean below 3000-m depth, the upward heat transport from the deep cell increases with increasing winds. This may indicate that as more heat is transported downward by the increasingly wind-forced thermally indirect deep cell, more heat is transported upward by the thermally direct bottom cell to compensate. Indeed, any heat transported downward by a thermally indirect circulation must be balanced, in steady state, by upward fluxes of heat by a thermally direct circulation and/or by subgrid-scale convective fluxes.

The total advective vertical heat transport reduces linearly with reducing wind stress in the model. Only in the TAU05 experiment is the total circulation net thermally direct in the manner proposed by classical models of the deep circulation (Munk 1966; Stommel and Arons 1960; Sandström 1908).

9. Discussion

While there are major advantages in averaging vertical transport in thermodynamic coordinates, a number of limitations remain in terms of their interpretation and comparison across models. First, some subgrid-scale processes in coarse-resolution models, such as convective mixing, may be substituted by eddy transport at higher resolution. Hence, the comparison between low and high resolution becomes somewhat ambiguous unless the subgrid fluxes are discussed alongside the transport from resolved circulation. In addition, as resolution increases, the role of resolved turbulent fluctuations becomes more apparent and hence the time scales over which the vertical transport is averaged become increasingly important.

A second caveat to this study is that the meridional overturning circulation in the North Atlantic in UVic ESM, at 13 Sv, is considerably weaker than that estimated from observations (18.7 Sv; Cunningham et al. 2007). This suggests that the role of the Atlantic overturning may be underestimated in our model and this may lead to an overly thermally indirect circulation.

A third and final caveat is that mesoscale eddies are likely to significantly compensate for the wind-forced component of the thermally indirect circulation in the Southern Ocean and changes therein (Zika et al. 2013). While parameterized eddy transport is included in all the diagnostics discussed here, this eddy transport is represented crudely in the model with a constant eddy mixing coefficient. Thus, analysis of a range of models with resolved eddies and more complex eddy parameterizations, employing the new diagnostic methods presented here, would aid in determining the possible nature of the vertical heat transport in the real ocean.

Some remarks are warranted with regard to the driving mechanisms of the surface cell. The surface cell is thermally direct, implying colder (and here denser) water downwells and warmer (lighter) water upwells (Figs. 2 and 6). This does not, however, necessarily imply that the cell is driven by buoyant processes; it merely implies that the cell could be driven by buoyant processes. It is unclear from the analysis discussed here whether the surface cell is in fact driven by buoyant processes or whether it is driven by low-latitude winds. Distinguishing the two mechanisms is left to future work. However, given strong wind-driven upwelling along the equator as a result of Ekman divergence and the well-established link between wind stress curl and the subtropical gyres (which are coincident with the water masses of the surface cell), the wind is likely to play a major role.

10. Summary and conclusions

Mechanisms of vertical advective heat transport have been investigated using a global climate model and novel thermodynamic methods. The thermal overturning streamfunction has been diagnosed and partitioned into thermally direct cells that flux heat upward and thermally indirect cells that flux heat downward. Using joint distribution functions for the vertical volume transport in temperature versus latitude coordinates, the latitudes at which up- and downwelling occurs in each cell can be identified. Likewise, using joint distributions in temperature and salinity coordinates, the salinity and density at which the cells up- and downwell can be diagnosed.

Three thermal overturning cells are identified in UVic ESM. They are a thermally direct bottom cell, a thermally indirect deep cell, and a thermally direct surface cell. The three cells correspond to the Antarctic Bottom Water circulation (also known as the lower cell of the meridional overturning), the pole-to-pole upper limb of the meridional overturning and the surface component of the subtropical gyres, respectively.

The deep cell is found to flux salt downward, suggesting that salinity gain near the surface makes its downwelling branch denser. This is consistent with the deep cell being part of a broader thermohaline circulation. By projecting the deep and surface cells into thermohaline coordinates, we find that both components make up the global cell of the thermohaline circulation identified by Zika et al. (2012) and Döös et al. (2012). Our analysis suggests that the salinity gain achieved by the deep cell occurs as a result of a transfer of freshwater from deep circulation to the subtropical gyres, and a transfer of more saline water from the gyres to the deep circulation through advection and/or diffusion.

In the model discussed, the deep cell fluxes dense water downward and light water upward in an integrated sense. Hence, the deep cell contributes to a gain in gravitational potential energy (Nycander et al. 2007). This implies that the thermally indirect deep cell requires a source of mechanical energy. Experiments with perturbed winds show an almost linear relationship between the strength of the deep cell and the Southern Hemisphere westerly wind stress. We thus conclude that a significant portion of ocean circulation can pump heat into the deep ocean, through a combination of haline and wind forcing.

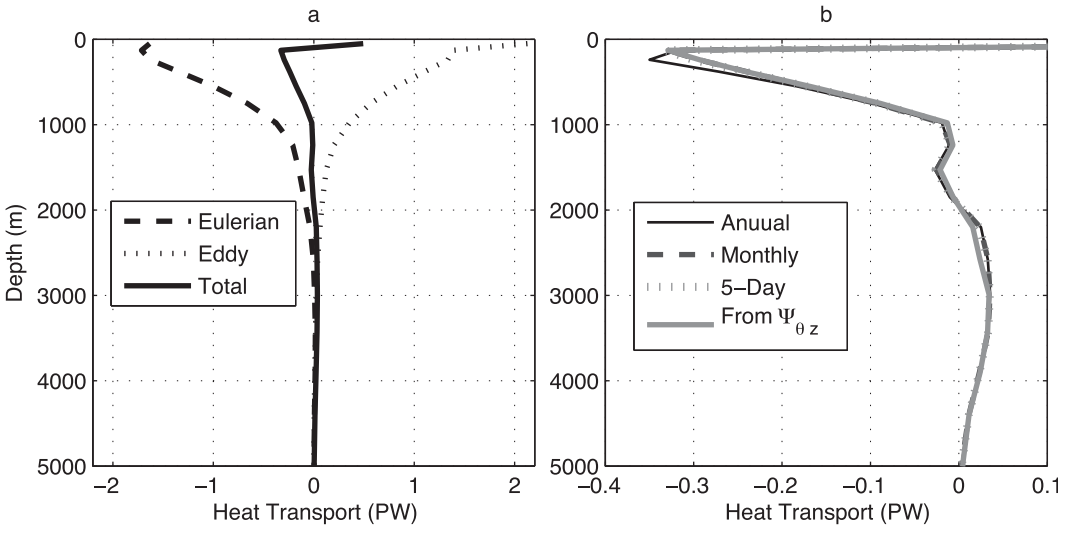

FIG. A1. (a) Vertical advective heat transport from the Eulerian- (black dashed) and eddy-induced (black dotted) velocity and the sum of the two (black solid) computed from monthly-mean fields. (b) Vertical heat transport given different sampling frequencies including annual- (black solid), monthly- (black dashed), and 5-day-average (gray dotted) values, and from the streamfunction $\Psi_{\theta z}$ derived using bin sizes of 0.1°C. In (b), the monthly- and 5-day-averaged transports are indistinguishable from one another on the scale shown.

Acknowledgments. This work was supported by the Australian Research Council. Jan Zika would like to acknowledge the support of a National Environment Research Centre Fellowship Grant. We thank Andy Hogg, Jonas Nycander, George Nurser, Jonathan Gregory, and an anonymous reviewer for providing helpful comments.

APPENDIX

The Influence of Sampling Frequency and Bin Size

Here, we discuss the influence of the Eulerian- and eddy-induced vertical velocity components, the sampling frequency, and the joint distribution bin size on the calculation of the advective vertical heat flux.

In UVic ESM, both the Eulerian- w^{Eul} and eddy-induced w^{Eddy} vertical velocity contributes to the vertical advective transport of tracers. The Eulerian velocity is derived from the horizontal divergence of the horizontal velocity that is solved within momentum equations. In the model, the eddy-induced vertical velocity results from the parameterization of Gent and McWilliams (1990) and is designed to account for the advective transport of water masses by mesoscale eddies that are not resolved on the coarse-resolution grid of the model (1.8° latitude by 3.6° longitude).

The vertical heat flux is computed for each component of the vertical velocity with monthly averaged output using

$$\frac{1}{\Delta t}\int_{t}^{t+\Delta t}\int_{-180^\circ}^{180^\circ}\int_{-90^\circ}^{90^\circ}\rho_0 C_p w\theta r^2\cos(y)\,dy\,dx\,dt. \qquad \text{(A1)}$$

The Eulerian vertical velocity contributes up to 1.7 PW of downward heat transport (at 150-m depth; Fig. A1a). This is compensated by up to 2.1 PW of upward heat flux by the eddy-induced velocity (at 50-m depth; Fig. A1a). The strong upward vertical heat flux resulting from eddies is consistent with the eddy-resolving model results of Wolfe et al. (2008) from the Parallel Ocean Program (POP) model.

In this study, monthly averaged fields are used to compute overturning streamfunctions and vertical advective property transport. Here, we test the sensitivity to the sampling frequency. The vertical heat transport is computed from (A1) using annual-, monthly-, and 5-day-average vertical velocities (the sum of Eulerian- and eddy-induced velocity in each case). These are shown in Fig. A1b. At 250-m depth, the downward vertical transport for annual-average sampling is approximately 0.05 PW more than the 5-day- and monthly-average value of 0.3 PW. The difference between monthly- and 5-day-average derived heat transport is negligible. Models that resolve mesoscale turbulence are likely to require a higher sampling frequency to the coarse-resolution model discussed here.

In section 4 and throughout this study, vertical heat transport is related to distribution functions. Distribution functions are calculated by summing the transport in terms of tracer value bins. The advective heat transport derived from the distribution function approaches

the exact advective heat transport value as the bin size approaches zero. In practice, we use a bin size for temperature of 0.1°C.

Here, we test the accuracy of this bin size by comparing the vertical heat transport derived from (A1) where no binning is required, with that derived from the thermal overturning streamfunction $\Psi_{\theta z}$, via (11) with a bin size of 0.1°C. Differences between the two calculations are negligible in the ocean above 2000-m depth. The sampling underestimates the upward heat transport by 0.01 PW at 2500-m but accurately captures the minimum at 3000-m depth.

REFERENCES

Andrews, D. G., and M. E. McIntyre, 1976: Planetary waves in horizontal and vertical shear: The generalized Eliassen–Palm relation and the zonal mean acceleration. *J. Atmos. Sci.,* **33,** 2031–2048.

Cunningham, S. A., and Coauthors, 2007: Temporal variability of the Atlantic meridional overturning circulation at 26.5°N. *Science,* **317,** 935–938.

Cuny, J., P. B. Rhines, P. P. Niiler, and S. Bacon, 2002: Labrador Sea boundary currents and the fate of the Irminger Sea water. *J. Phys. Oceanogr.,* **32,** 627–647.

Domingues, C. M., J. A. Church, N. J. White, P. J. Gleckler, S. E. Wijffels, P. M. Barker, and J. R. Dunn, 2008: Improved estimates of upper-ocean warming and multidecadal sea level rise. *Nature,* **453,** 1090–1093.

Döös, K., J. Nilsson, J. Nycander, L. Brodeau, and M. Ballarotta, 2012: The World Ocean thermohaline circulation. *J. Phys. Oceanogr.,* **42,** 1445–1460.

Eden, C., R. J. Greatbatch, and D. Olbers, 2007: Interpreting eddy fluxes. *J. Phys. Oceanogr.,* **37,** 1282–1296.

England, M. H., 1995: The age of water and ventilation timescales in a global ocean model. *J. Phys. Oceanogr.,* **25,** 2756–2777.

Ferrari, R., and D. Ferreira, 2011: What processes drive the ocean heat transport. *Ocean Modell.,* **38,** 171–186.

Gent, P. R., and J. C. McWilliams, 1990: Isopycnal mixing in ocean circulation models. *J. Phys. Oceanogr.,* **20,** 150–155.

Gerdes, R., C. Köberle, and J. Willebrand, 1991: The influence of numerical advection schemes on the results of ocean general circulation models. *Climate Dyn.,* **5,** 211–226.

Gill, A. E., 1982: *Fundamentals of Ocean Climate Models.* Academic Press, 662 pp.

Gnanadesikan, A., R. D. Slater, P. S. Swathi, and G. K. Vallis, 2005: The energetics of ocean heat transport. *J. Climate,* **18,** 2604–2616.

Gregory, J. M., 2000: Vertical heat transports in the ocean and their effect on time-dependent climate change. *Climate Dyn.,* **16,** 501–515.

Held, I. M., M. Winton, K. Takahashi, T. Delworth, F. Zeng, and G. K. Vallis, 2010: Probing the fast and slow components of global warming by returning abruptly to preindustrial forcing. *J. Climate,* **23,** 2418–2427.

Jayne, S. R., and J. Marotzke, 2002: The oceanic eddy heat transport. *J. Phys. Oceanogr.,* **32,** 3328–3345.

Kalnay, E., and Coauthors, 1996: The NCEP/NCAR 40-Year Reanalysis Project. *Bull. Amer. Meteor. Soc.,* **77,** 437–471.

Laliberté, F., T. Shaw, and O. Pauluis, 2012: Moist recirculation and water vapor transport on dry isentropes. *J. Atmos. Sci.,* **69,** 875–890.

Marsh, R., S. A. Josey, A. J. G. de Nurser, B. A. Cuevas, and A. C. Coward, 2005: Water mass transformation in the North Atlantic over 1985–2002 simulated in an eddy-permitting model. *Ocean Sci.,* **1,** 127–144.

McDougall, T. J., 2003: Potential enthalpy: A conservative oceanic variable for evaluating heat content and heat fluxes. *J. Phys. Oceanogr.,* **33,** 945–963.

——, and P. C. McIntosh, 1996: The temporal-residual-mean velocity. Part I: Derivation and the scalar conservation equations. *J. Phys. Oceanogr.,* **26,** 2653–2665.

Munk, W. H., 1966: Abyssal recipes. *Deep-Sea Res.,* **13,** 707–730.

Nurser, A. J. G., and M.-M. Lee, 2004: Isopycnal averaging at constant height. Part I: The formulation and a case study. *J. Phys. Oceanogr.,* **34,** 2721–2739.

Nycander, J., J. Nilsson, K. Döös, and G. Bromström, 2007: Thermodynamic analysis of ocean circulation. *J. Phys. Oceanogr.,* **37,** 2038–2052.

Pacanowski, R., 1995: MOM2 documentation users guide and reference manual. GFDL Ocean Group Tech. Rep. 3.2, 232 pp.

Pauluis, O., A. Czaja, and R. Korty, 2008: The global atmospheric circulation on moist isentropes. *Science,* **321,** 1075.

——, T. Shaw, and F. Laliberté, 2011: A statistical generalization of the transformed Eulerian-mean circulation for an arbitrary vertical coordinate system. *J. Atmos. Sci.,* **68,** 1766–1783.

Sandström, J. W., 1908: Dynamische Versuche mit Meerwasser. *Ann. Hydrogr. Martimen Meteor.,* **36,** 6–23.

Sijp, W. P., and M. H. England, 2009: Southern Hemisphere westerly wind control over the ocean's thermohaline circulation. *J. Climate,* **22,** 1277–1286.

——, M. Bates, and M. H. England, 2006: Can isopycnal mixing control the stability of the thermohaline circulation in ocean climate models? *J. Climate,* **19,** 5637–5651.

Solomon, S., D. Qin, M. Manning, M. Marquis, K. Averyt, M. M. B. Tignor, H. L. Miller Jr., and Z. Chen, Eds., 2007: *Climate Change 2007: The Physical Science Basis.* Cambridge University Press, 996 pp.

Stommel, H., and A. B. Arons, 1960: On the abyssal circulation of the world's ocean–II. An idealized model of circulation pattern and amplitude in oceanic basins. *Deep-Sea Res.,* **6,** 140–154.

Toggweiler, J. R., and B. Samuels, 1995: Effect of Drake Passage on the global thermohaline circulation. *Deep-Sea Res.,* **42,** 477–500.

Weaver, A. J., and Coauthors, 2001: The UVIC earth system climate model: Model description, climatology, and applications to past, present, and future climates. *Atmos.–Ocean,* **39,** 361–428.

Wolfe, C., P. Cessi, J. McClean, and M. Maltrud, 2008: Vertical heat transport in eddying ocean models. *Geophys. Res. Lett.,* **35,** L23605, doi:10.1029/2008GL036138.

Zika, J. D., M. H. England, and W. P. Sijp, 2012: The ocean circulation in thermohaline coordinates. *J. Phys. Oceanogr.,* **2,** 708–724.

——, and Coauthors, 2013: Vertical eddy fluxes in the Southern Ocean. *J. Phys. Oceanogr.,* **43,** 941–955.